Plectin-containing, centrally localized focal adhesions exert traction forces in primary lung epithelial cells

Jessica L. Eisenberg[1], Kristin G. Beaumont[1,2], Desire Takawira[1], Susan B. Hopkinson[1], Milan Mrksich[1,2], G. R. Scott Budinger[1,3] and Jonathan C. R. Jones[1,*]

[1]Department of Cell and Molecular Biology, Northwestern University, Chicago, IL, USA
[2]Departments of Chemistry and Biomedical Engineering, and Howard Hughes Medical Institute, Northwestern University, Evanston, IL, USA
[3]Department of Medicine, Feinberg School of Medicine, Northwestern University, Chicago, IL, USA
*Author for correspondence (j-jones3@northwestern.edu)

Accepted 13 May 2013
Journal of Cell Science 126, 3746–3755

doi: 10.1242/jcs.128975

Summary

Receptor clustering upon cell attachment to the substrate induces assembly of cytoplasmic protein complexes termed focal adhesions (FAs), which connect, albeit indirectly, the extracellular matrix to the cytoskeleton. A subset of cultured primary alveolar epithelial cells (AEC) display a unique pattern of vinculin/paxillin/talin-rich FAs in two concentric circles when cultured on glass and micropatterned substrates: one ring of FAs located at the cell periphery (pFAs), and another FA ring located centrally in the cell (cFAs). Unusually, cFAs associate with an aster-like actin array as well as keratin bundles. Moreover, cFAs show rapid paxillin turnover rates following fluorescence recovery after photobleaching and exert traction forces similar to those generated by FAs at the cell periphery. The plakin protein plectin localizes to cFAs and is normally absent from pFAs, whereas tensin, a marker of mature/fibrillar adhesions, is found in both cFAs and pFAs. In primary AEC in which plectin expression is depleted, cFAs are largely absent, with an attendant reorganization of both the keratin and actin cytoskeletons. We suggest that the mechanical environment in the lung gives rise to the assembly of unconventional FAs in AEC. These FAs not only show a distinctive arrangement, but also possess unique compositional and functional properties.

Key words: Focal adhesion, Cytoskeleton, Alveolar epithelial cells, Traction force

Introduction

Adhesion of mammalian cells is mediated by receptor interaction with extracellular matrix (ECM) components along regions of cell–substrate attachment (Berrier and Yamada, 2007; Burridge et al., 1988; Zamir and Geiger, 2001). The molecular components of matrix attachment sites are numerous, with the proteins comprising the 'adhesome' complex numbering over 150 (Geiger and Zaidel-Bar, 2012; Zaidel-Bar et al., 2007). Adhesome structures are generally classified into three types (Zaidel-Bar et al., 2004; Zamir and Geiger, 2001; Zamir et al., 1999). Focal complexes assemble after initial contact between receptors and ECM at the leading edge, or lamellipodium, of a migrating cell. The focal complex is a small (~0.25 μm^2), dot-like structure comprising integrins, talin and focal adhesion kinase (FAK) (Lawson et al., 2012; Zamir and Geiger, 2001; Zamir et al., 1999). As the lamellipodium advances, new focal complexes are formed while the original complexes mature into focal adhesions (FAs). FAs differ from focal complexes by being larger (~1–2 μm^2) structures, by exhibiting higher levels of phosphotyrosine and by containing additional components including paxillin, vinculin and zyxin. Assembly of actin bundles at these sites is concomitant with the transition from focal complexes to FAs. Indeed, the presence of mechanical force due to actomyosin-driven contractility has been reported to be a key factor in FA maturity (Geiger and Bershadsky, 2001; Riveline et al., 2001). Subsequently, FAs translocate centripetally and recruit tensin (Zamir et al., 2000). These tensin-containing clusters have been termed fibrillar adhesions, appear as elongated fibrils or arrays of dots with a distribution in the central zone and are enriched in $\alpha5\beta1$ integrin, actin and fibrils of fibronectin, but contain little phosphotyrosine or other FA proteins (Zamir et al., 1999).

Within the lung, alveolar epithelial cells (AEC) are responsible for gas exchange and are exposed to mechanical forces, including deformation/strain during normal breathing and shear stress during the distension of the airway walls and blood vessels from air and blood flow (Liu et al., 1999; Wirtz and Dobbs, 2000). Specifically, normal respiration involves the uniform transmission of negative pleural pressures to the individual alveolar units, allowing for their uniform expansion and contraction during each respiratory cycle (Mead et al., 1970). We reasoned that the unique mechanical requirements of the lung might be reflected in unusual adherence of individual epithelial cells. Indeed, here we describe a highly unusual form and pattern of FAs in a subset of primary AEC. These AEC assemble a unique arrangement of FAs in a circular fashion in the central region of the cell (cFAs) as well as another set of FAs along the cell periphery (pFAs). We find the fibrillar adhesion marker tensin as well as talin, paxillin and vinculin are all found in both sets of FAs. However, the cytolinker plectin is enriched only in cFAs, and a loss of plectin significantly reduces the number of cells displaying this unique FA double ring arrangement. Intriguingly, in AEC plated onto micropatterned surfaces, cFAs assemble in an arrangement that mirrors a wide variety of cell shapes. Moreover, cFAs in primary AEC not only restrain the actin and keratin intermediate filaments but also, unexpectedly, display

more dynamic properties than pFAs as assessed by fluorescence recovery after photobleaching (FRAP) and exert traction forces comparable to FAs at the cell edge. Our results describe a unique class of FAs present in AEC that break some of the rules of traditional FAs.

Results

Primary AEC display unique arrangement of FAs

To determine how FAs are organized in AEC, we immunostained primary rat AEC (rAEC) maintained on glass coverslips for vinculin, paxillin and talin (Fig. 1A,B). We found a subpopulation of rAEC display FAs in two concentric circles (25.1±10.3% of cells, n=444 total cells counted in groups of eight or less in three separate experiments; Fig. 1C). One circle of FAs locates near the cell periphery (pFAs) while the other occurs towards the central region of the cell (cFAs). These two rings of FAs are observed in cells with at least one free edge, with the pattern being more pronounced in single cells (Fig. 1A,B). In the remaining population of rAEC, some FAs locate at the cell edges while others show a random distribution over the entire interior, cell–substrate interface of the cells (Fig. 1A,B). By culturing the cells overnight in reduced calcium media to decrease assembly of cell–cell junctions, the number of cells exhibiting the FA double ring pattern increases 1.5-fold, to 37.6±2.1% (n=247 cells) when compared to cells cultured in normal media (Fig. 1C; supplementary material Fig. S1A).

In rAEC, both pFAs and cFAs contain paxillin, vinculin and talin (Fig. 1A,B). We screened for additional proteins to better characterize these adhesions. We stained for the cytolinker protein plectin, which our previous data indicated is a key mediator of AEC mechanosignaling present in FAs (Takawira et al., 2011). Plectin is also a component of FAs of various fibroblasts, epithelial

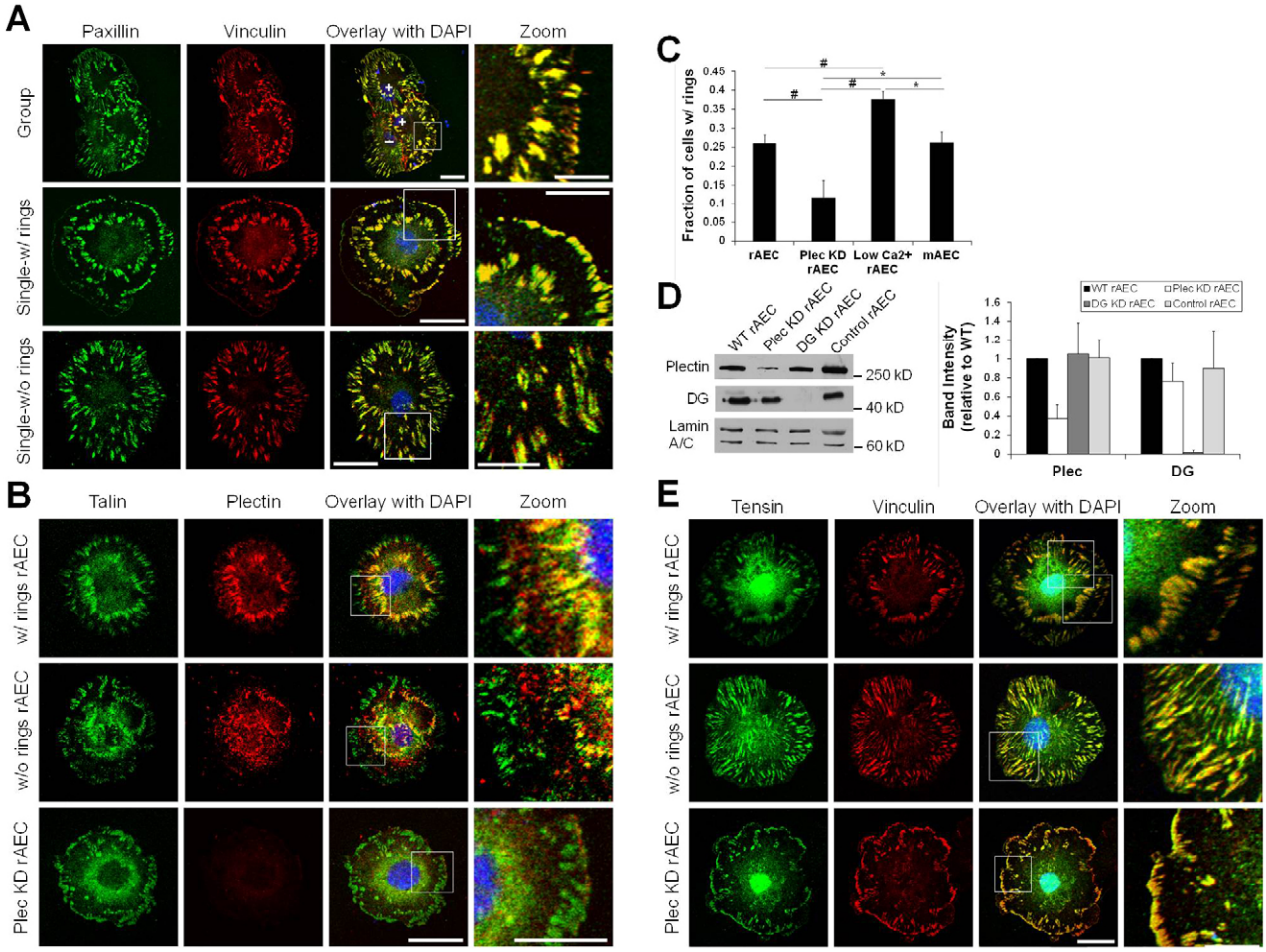

Fig. 1. FA organization in alveolar epithelial cells. (**A**,**B**,**E**) Primary rAEC maintained on glass coverslips were immunostained with combinations of antibodies against vinculin, paxillin, talin, plectin or tensin, as indicated. The overlays of the two left columns of images are shown in the third column and include nuclear DAPI staining. The boxed areas in the overlays are shown at higher magnifications in the right column (zoom). Images of cells exhibiting double FA rings (w/ rings) and those that do not (w/o rings) are presented. (**C**) Percentage of rAEC, Plec KD rAEC, rAEC maintained overnight in low calcium medium (low Ca^{2+} rAEC), and mAEC exhibiting double rings of FAs. Data are presented as the mean percentage (± s.d.) of cells displaying FAs in the double ring pattern out of total cells counted per condition; n>200 cells immunostained with FA proteins in two or three separate experiments. *P<0.05; $^{\#}P$<0.01. (**D**) Extracts of uninfected, wild-type rAEC and rAEC infected with viruses encoding rat-specific plectin (Plec KD), rat-specific dystroglycan (DG KD) or human-specific control shRNAs were immunoblotted using antibodies against plectin, DG or lamin A/C. Immunoblots were scanned densitometrically, and the levels of plectin and DG were calculated relative to the levels in wild-type rAEC. The graph shows average blot densities for ≥3 different samples per condition (± s.d.). Scale bars: 20 μm in the overlay; 10 μm in zoom.

and endothelial cells and is also found in epithelial matrix junctions termed hemidesmosomes (Bhattacharya et al., 2009; Burgstaller et al., 2010; Seifert et al., 1992; Tsuruta et al., 2002; Wiche, 1998). We found plectin enriched in cFAs, where it co-localizes with talin, but is mostly absent from pFAs (Fig. 1B). Similarly, in rAEC without double FA rings, we observe some plectin co-localization with talin in interior FAs, although not to the same degree as in cells with rings, while plectin is absent from FAs at the cell periphery (Fig. 1B).

We next determined if the formation of cFAs in primary rAEC is common to all lung epithelial cells. We analyzed FAs in primary mouse AEC (mAEC) as well as immortalized mouse and rat epithelial cells derived from lung alveoli (MLE 12 and RLE-6TN cells respectively). A subset of mAEC possesses double rings of FAs, with talin and plectin co-localizing in cFAs in these cells (Fig. 1C; supplementary material Fig. S1A). However, neither MLE 12 nor RLE-6TN cells display a similar FA arrangement (supplementary material Fig. S1A). In RLE-6TN cells, plectin and talin poorly co-distribute in random FAs located within the cell but not at the periphery, whereas plectin in MLE 12 cells shows limited co-localization with talin in some FAs located close to the cell edge (supplementary material Fig. S1A). Indeed, in these cells plectin primarily appears diffusely distributed or, possibly, colocalized with the filamentous cytoskeleton (supplementary material Fig. S1). We also stained other epithelial cell lines (804G, rat bladder epithelial cells and HEK, human epidermal keratinocytes) with talin and plectin antibodies and observed no co-localization of the two proteins (supplementary material Fig. S1A). Instead, in both of these cell lines, talin localizes to small FAs at the cell periphery, while plectin is found in hemidesmosome protein rich spots or arc structures as detailed by us previously (Hamill et al., 2009; Riddelle et al., 1991). These data indicate that the formation of plectin-rich cFAs is particular to primary AEC.

FA double ring formation is plectin dependent

The enrichment of plectin in the cFAs of primary AEC led us to investigate whether plectin is necessary for their formation. Using adenoviral infection of plectin shRNA, we achieved ~65% knockdown of plectin in rAEC after 48 hours (Takawira et al., 2011) (Fig. 1D). There is no difference in the number of cells displaying FAs in a double ring pattern in AEC infected with adenovirus encoding dystroglycan (DG KD) or control shRNAs. However, the percentage of rAEC infected with plectin shRNA (Plec KD) exhibiting the double rings of FAs is reduced to 11.7±4.5% (n=355 cells; Fig. 1C). The FAs in Plec KD rAEC primarily localize to the cell periphery, with fewer internal FAs observed than in control cells, regardless of whether the latter possess or lack FA double rings (Fig. 1E). Additionally, there is an increase in the number of larger FAs in Plec KD rAEC versus controls (supplementary material Fig. S1B). Knocking down plectin in the RLE-6TN cells results in a similar increase in the numbers of large FAs at the cell edge as well as a loss of interior FAs (supplementary material Fig. S1A). Conversely, plectin knock-down results in little, if any, change in the distribution or size of FAs in 804G cells (supplementary material Fig. S1A).

The cFAs in the inner ring in rAEC are not traditional fibrillar adhesions

The cFAs in rAEC localize to the same cell region as fibrillar adhesions in other cell types (Zamir et al., 1999; Zamir et al., 2000). To assess whether they are traditional fibrillar adhesions, rAEC were stained for tensin, a fibrillar adhesion marker. Remarkably, tensin localizes to both pFAs and cFAs of rAEC (Fig. 1E). Moreover, tensin is also present in the large FAs towards the cells edge of Plec KD rAEC (Fig. 1E). Control shRNA has no impact on tensin organization in cells with and without the double FA rings (not shown).

The cFAs in the inner ring in rAEC influence actin cytoskeletal organization

FAs organize the actin cytoskeleton (Burridge and Chrzanowska-Wodnicka, 1996; Geiger and Bershadsky, 2001; Geiger et al., 2009). In rAEC displaying the FA double ring pattern, actin bundles arrange in a highly unusual fashion (Fig. 2A). One set of actin bundles encircles the cell periphery and is associated with pFAs. A second set of thick actin bundles occurs at the center of the cell in a starburst or aster-like array. These bundles terminate at cFAs. Few, if any, bundles connect the inner and outer rings of FAs. rAEC without FA rings display thick actin bundles encircling the cell periphery, with a few filaments connecting FAs throughout the cell, but no aster-like organization is detected (Fig. 2A). In Plec KD rAEC, actin bundles mainly localize to the large FAs at the cell edge, also with no aster-like central actin array (Fig. 2A). mAEC exhibit the same FA and actin arrangement as their primary rat counterparts, whereas MLE 12, RLE-6TN, 804G and HEK cells do not (supplementary material Fig. S2A).

In order to quantify the differences in the actin arrangements in rAEC which possess double rings with those rAEC which do not, we first performed single line scan fluorescence intensity measurements (Fig. 2B; based on the white lines drawn through actin stained images in Fig. 2A). The plot of the line scans clearly shows the dramatic increase in central actin fluorescence intensity in rAEC with rings compared to rAEC without rings. Also from these plots, we observe that rAEC without rings display thicker regions of actin bundles at the cell periphery versus those cells with rings. Therefore, we also measured the thickness of the actin bundles at the cell edge in rAEC with and without rings. We found that wild-type rAEC without rings display significantly thicker actin bundles around the cell periphery than rAEC with rings (Fig. 2C). Additionally, wild-type rAEC without rings also exhibit significantly thicker actin bundles at the cell edge than Plec KD rAEC (Fig. 2C).

Next, we determined if the different actin organizations display different levels of contractility by staining rAEC with antibodies against phosphorylated and total myosin. We observe phosphorylated myosin with both the actin bundles at the cell periphery as well as the aster-like actin arrangement, indicating both actin arrangements are contractile (Fig. 2D). Additionally, cells lacking the inner aster-like actin also show phosphorylated myosin in the thick actin bundles at the cell periphery, but there is little staining for phospho-myosin within the cell interior (Fig. 2D). In contrast, antibodies against phospho-myosin co-stain actin fibers spanning the interior cytoplasm of RLE-6TN cells (supplementary material Fig. S2B).

We next asked whether the formation of a cFA ring and the distinct actin cytoskeletal organization in rAEC is influenced by cell shape and/or contractility. We took advantage of a micropatterning technique to create arrayed substrates composed of uniform, single cell-sized fibronectin adhesive areas with defined geometric cues (Chen et al., 1998; Ostuni et al., 2009). This method provides a way to control size, curvature,

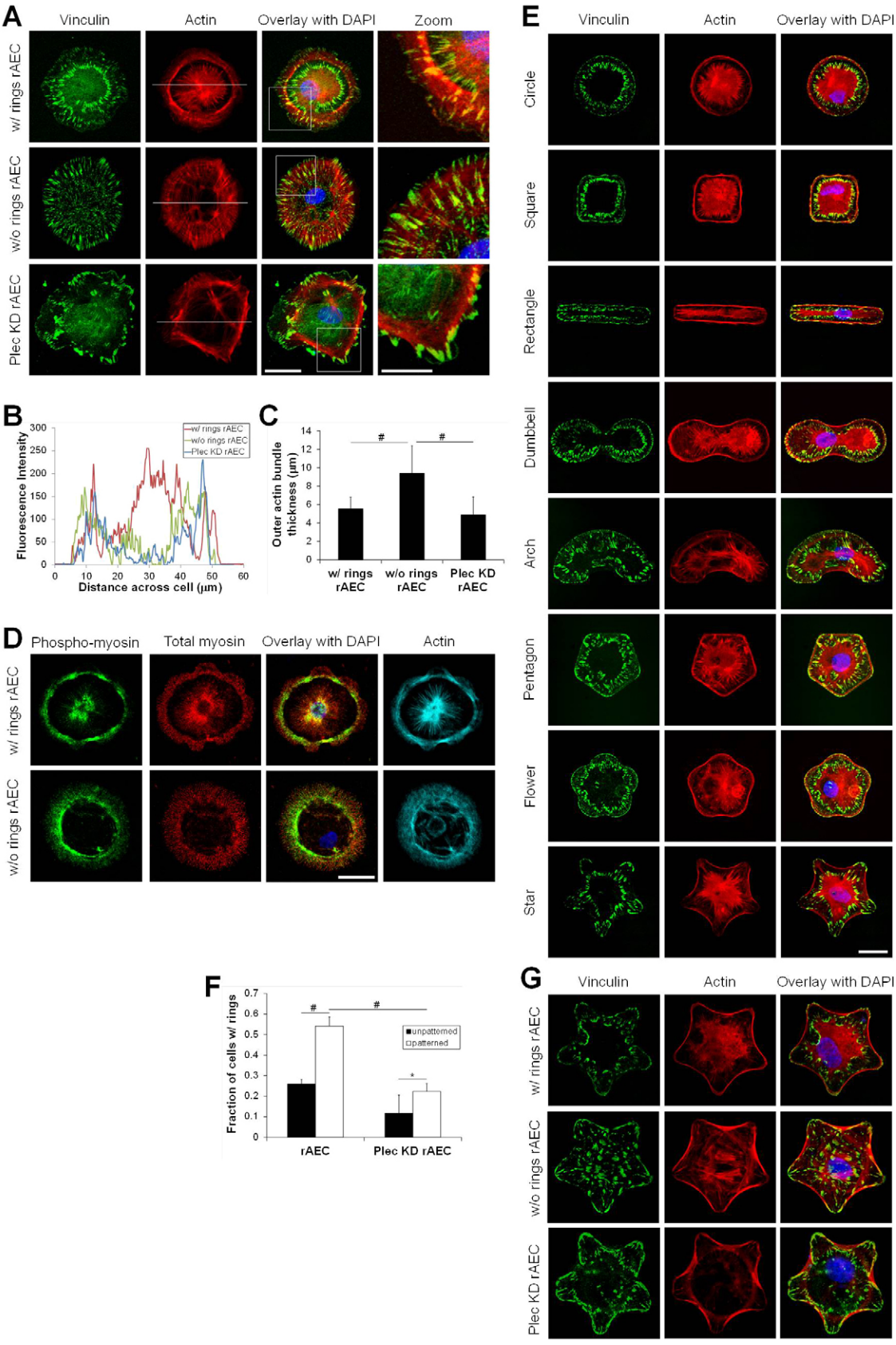

Fig. 2. See next page for legend.

tension and polarity of a cell to assess how these properties influence cellular processes such as attachment, apoptosis, migration and differentiation (Bhadriraju et al., 2007; Brock et al., 2003; Chen et al., 1997; Dike et al., 1999; James et al., 2008; Kilian et al., 2010; McBeath et al., 2004). We seeded rAECs onto several differently shaped micropatterned substrates where each shape had an adhesive area of ~1000 μm^2 (Fig. 2E). An average of 54.1±8.9% of rAEC on micropatterned substrates (n>200 cells maintained for circle, square, rectangle and star micropatterns) display a double concentric organization of FAs and the corresponding central actin aster-like arrangement, a 2.1-fold increase from rAEC on unpatterned substrates (Fig. 2F). Moreover, in cells on each pattern studied, the organization of cFAs mirrors cell shape (Fig. 2E).

Given that we saw no influence of cell shape on the formation of the inner FA ring, we focused our subsequent studies using cells maintained on star micropatterns. Compared to the corresponding wild-type rAEC, the number of cells with the FA double ring and aster-like actin cytoskeleton arrangements is decreased 2.4-fold in Plec KD rAEC plated onto such a micropattern (22.3±3.8% for n=693 total cells counted) (Fig. 2F,G). These cells display mostly large FAs and actin bundles near the cell edge, similar to what we observed in cells maintained on unpatterned substrates (Fig. 2G). We also found that mAEC plated onto star micropatterned substrates exhibit both pFAs and cFAs, with the latter being the termination site for the bundles emanating from the central actin aster-like array as in rAEC (supplementary material Fig. S2C). Culturing MLE 12, RLE-6TN, 804G and HEK cells on the star micropatterns fails to induce such an organization of FAs and actin (supplementary material Fig. S2C).

The cFAs in the inner ring in rAEC are involved in keratin cytoskeleton organization

Plectin binds intermediate filament (IF) proteins and is involved in linking IFs to the cell surface (Bhattacharya et al., 2009; Burgstaller et al., 2010; Geerts et al., 1999; Gonzales et al., 2001; Karashima et al., 2012; Svitkina et al., 1996; Wiche, 1998). Additionally, there is precedence for FAs being important for IF organization (Bhattacharya et al., 2009; Burgstaller et al., 2010; Windoffer et al., 2006). Thus, we next determined if the plectin-containing cFAs influence the distribution of the IF keratin cytoskeleton of rAEC (Eisenberg et al., 2011; Takawira et al., 2011). In rAEC exhibiting rings of cFAs and pFAs, keratin bundles are restricted to the central cell area and closely associate with cFAs (Fig. 3A). Only a few thin keratin bundles are observed between the cFAs and pFAs. However, in wild-type and Plec KD rAEC, which do not display FA rings, the keratin bundles are located throughout the cell and commonly reach the cell periphery (Fig. 3A). In rAEC on micropatterned substrates which exhibit double rings, keratin bundles associate with or are close by cFAs (Fig. 3B; supplementary material Fig. S3). Similar to unpatterned cells, when maintained on patterned substrate, wild-type and Plec KD rAEC without double rings display a

Fig. 2. FA double rings influence actin cytoskeletal organization in AEC. In A,D,E and G overlays of the two left columns of images are shown in the third column and include DAPI staining of nuclei. (**A**) rAEC and Plec KD rAEC were prepared for immunostaining using an antibody against vinculin together with Rhodamine-conjugated phalloidin as a marker for actin. The boxed areas in the overlays are shown at higher magnifications in the column at the right (zoom). (**B**) Fluorescent profiles were generated across the cells at the position indicated by the white lines in the actin images in A. (**C**) The average thickness of the outer actin bundles was determined by measuring the actin fluorescence in four places across at least seven cells using images of actin staining similar to those shown in A. Values are the average thickness ± s.d.; $^{\#}P$<0.01. (**D**) rAEC plated on glass coverslips were processed for immunofluorescence with antibodies against phospho-myosin and total-myosin, and simultaneously stained with an Alexa-Fluor-647-conjugated phalloidin to mark the actin cytoskeleton. The images in the right column show the phalloidin stain for actin. (**E**) rAEC were plated onto various fibronectin-coated, micropatterned substrates and prepared for staining as indicated. (**F**) Percentage of rAEC and Plec KD rAEC showing rings after plating on micropatterned substrates compared with unpatterned substrates (see also Fig. 1B for unpatterned). n>100 cells immunostained with FA proteins counted on four different patterns in two or three separate experiments. Data are the percentage of cells containing the double ring FA pattern out of total cells counted per condition (average ± s.d.). *P<0.05; $^{\#}P$<0.01. (**G**) rAEC and Plec KD rAEC were plated on star-shaped patterns and stained to show vinculin and actin. Scale bars: 20 μm in the overlay; 10 μm in zoom.

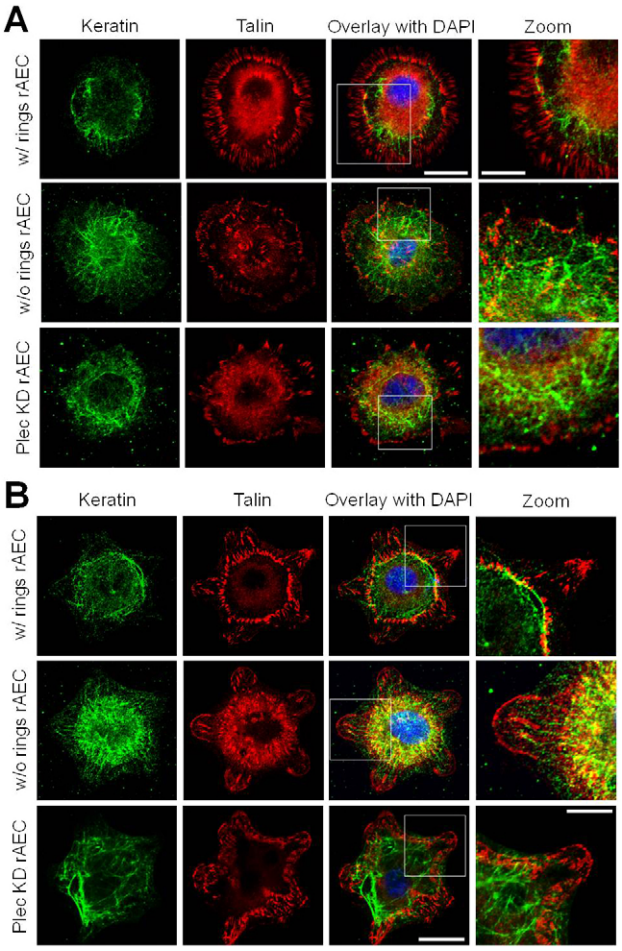

Fig. 3. Keratin intermediate filaments organize relative to the double rings of FAs in rAEC. (**A**) rAEC and Plec KD rAEC on glass coverslips were immunostained for talin and keratin as indicated. (**B**) rAEC and Plec KD rAEC were maintained on star micropatterned substrates and also stained for talin and keratin. Overlays of the two left columns of images are shown in the third column and include DAPI staining of nuclei. The boxed areas in overlays are shown at higher magnifications in the images on the right (zoom). Images of cells exhibiting double FA rings (w/rings) and those that do not (w/o rings) are presented. Scale bars: 20 μm in overlay; 10 μm in zoom.

reduction in keratin bundling (Fig. 3B; supplementary material Fig. S3). Furthermore, in such cells, there are numerous wispy keratin fibers scattered throughout the cytoplasm including some reaching the cell periphery (Fig. 3A,B; supplementary material Fig. S3).

The formation of cFAs requires cellular tension and contractility

The effects of micropatterned substrates on rAEC shape allowed us to assess tension and contractility requirements necessary for maintaining the FA double ring pattern. rAEC on star micropatterns were treated with cytochalasin D, blebbistatin, Y-27632, nocodazole or PF-573228 to perturb actin polymerization, myosin II-mediated contractility, microtubule polymerization and focal adhesion kinase (FAK) respectively. Since these treatments inhibit cell spreading, rAEC were seeded onto substrates and then treated with drugs 24 hours later. When the actin cytoskeleton is depolymerized by cytochalasin D and when contractility is inhibited by blebbistatin or Y-27632, the FA double ring in rAECs is not observed. In the treated cells, FAs are reduced in number and randomly scattered throughout the cell with the central actin aster also being missing (Fig. 4A). Microtubule depolymerization and FAK inhibition by nocodazole and PF-573228, respectively, have no effect on the numbers of cells exhibiting cFAs. In addition, keratin bundling in the central zone is lost in rAEC treated with cytochalasin D and blebbistatin (Fig. 4B).

cFAs show dynamic properties

We next compared the dynamics of pFAs and cFAs using GFP–paxillin-expressing rAEC since it has been previously reported that paxillin-containing FAs and tensin-containing fibrillar adhesions are highly dynamic (Zamir et al., 2000). First, we tracked the dynamics of GFP–paxillin by imaging cells for 20 minutes (supplementary material Fig. S4) (Ozawa et al., 2010; Tsuruta et al., 2002; Tsuruta et al., 2011). Surprisingly, we observe no dynamic movement of the cFAs, and pFAs display only limited centripetal movement (supplementary material Fig. S4). However, FRAP indicates that paxillin exchange in cFAs within the double ring is significantly faster than pFAs, where cFAs reach 50% recovery after about 25 seconds compared to 50 seconds in pFAs (Fig. 5). Comparably, FAs in rAEC without rings and RLE-6TN cells reach 50% recovery after 50–60 seconds, indicating cFAs in rings are more dynamic in this assay than those FAs as well (Fig. 5).

cFAs exert traction force

FAs exert traction forces, with recent data indicating that FAs at the cell edge support more tension than matrix adhesions located towards the cell center (Legant et al., 2013; Stricker et al., 2011). Given the unique nature of the cFAs, we decided to compare central and peripheral traction forces in rAEC with and without rings as well as RLE-6TN cells expressing GFP-tagged paxillin (Fig. 6A). In RLE-6TN cells, the ratio of forces elicited by internal FAs/peripheral FAs is close to 0, indicating that the FAs at the cell edge support more tension than the adhesions toward the cell center (Fig. 6B). In contrast, cFAs in rAEC support significant traction forces. In many cells, the ratio of forces elicited by cFAs/pFAs is >1 (Fig. 6B). This is not dependent on the rAEC assembling an inner ring of cFAs since we observe similar results when we analyze AEC that fail to assemble double

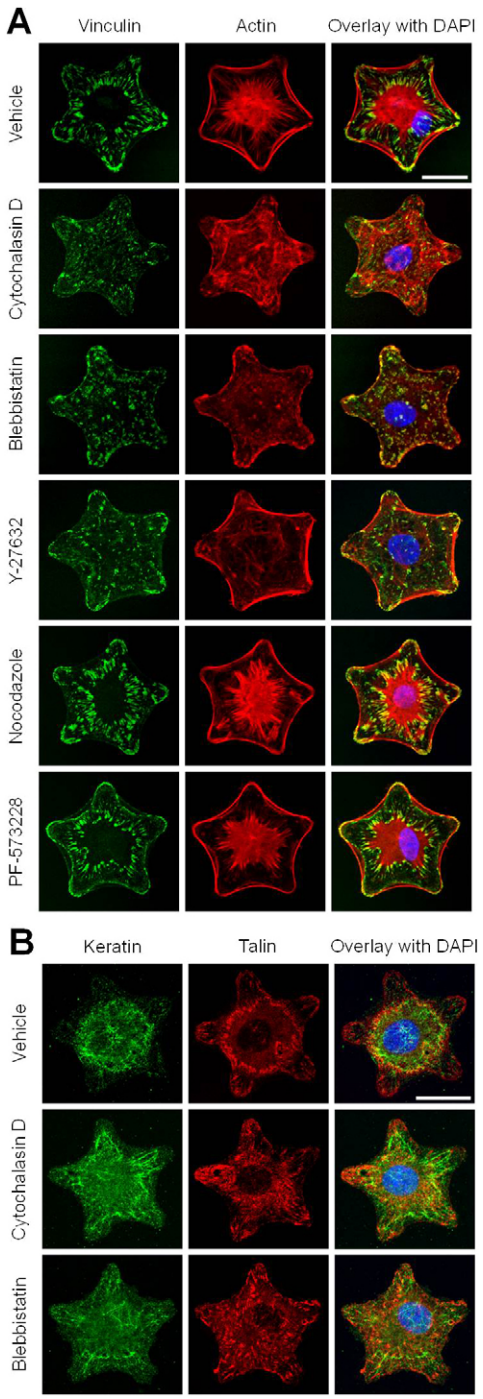

Fig. 4. Formation of double FA rings requires actin and myosin-dependent contractility. (**A**) rAEC were plated onto star micropatterned substrates and treated 24 hours later with various cytoskelon-disrupting drugs as indicated, before staining for vinculin and actin. 'Vehicle' indicates cells treated with DMSO alone. (**B**) Cells treated with vehicle, cytochalasin D and blebbistatin were also stained for keratin and talin. For A and B overlays of the two left columns of images are shown in the third column and include DAPI staining of nuclei. Scale bars: 20 μm.

rings of FAs. Indeed, this unusual force-bearing behavior distinguishes the cFAs in rings and the interior FAs of AEC from interior FAs in other cell types (Stricker et al., 2011). We also compared overall traction forces in rAEC versus Plec KD

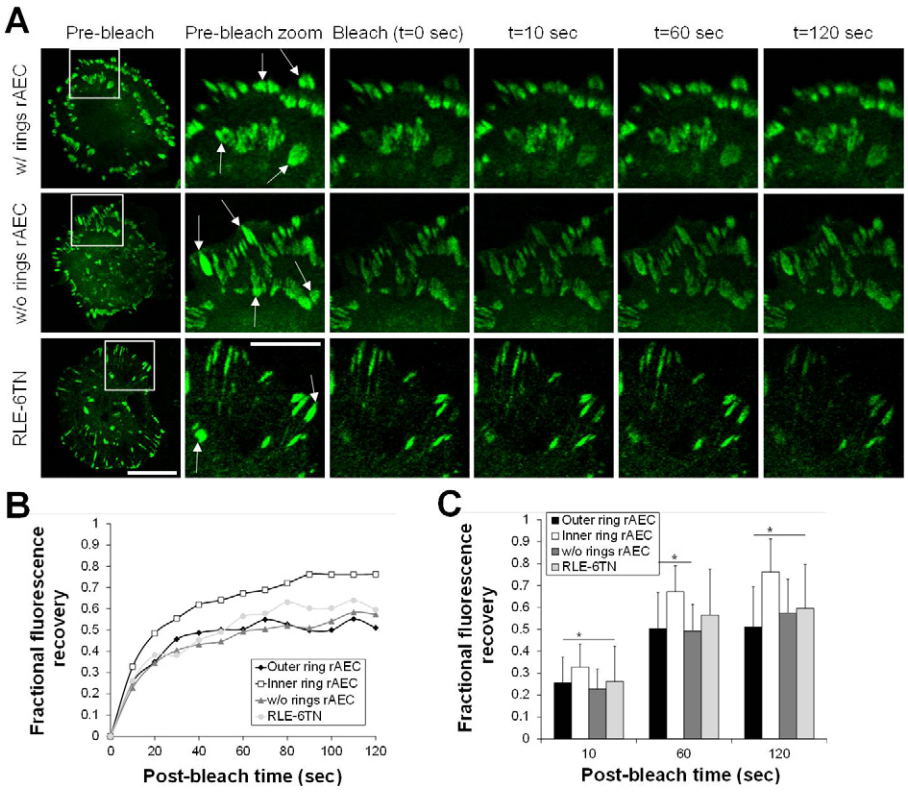

Fig. 5. The cFAs within the double ring exhibit faster turnover than pFAs following fluorescence recovery after photobleaching. (**A**) rAEC both with and without the double ring FA pattern as well as RLE-6TN cells expressing GFP–paxillin were subjected to FRAP (bleached areas indicated with arrows in zoomed images designated with white box in whole cell pre-bleach images). Images of the cells were collected every 10 seconds following photobleaching to monitor the recovery of the fluorescence signal. (**B**) Fluorescence recovery occurs faster in cFAs in rAEC with the double ring pattern. FRAP data were quantified for five to seven cells per type, with two to six FAs bleached per cell. Data are the average fluorescence recovery values for each time point. (**C**) Selected time points from the data presented in B were plotted to show the average fluorescence recovery (± s.d.) in each cell type; $*P<0.05$. Scale bars: 20 μm in pre-bleach; 10 μm in zoom.

rAEC and, not surprisingly, we observe a decrease in forces in the Plec KD rAEC, consistent with results reported for other cell types (Fig. 6C) (Na et al., 2009).

Discussion

Our results indicate that a subset of primary AEC (~25%) display a novel, highly unusual, pattern of FAs in two concentric circles, one at the periphery and one within the central region of the cell. In addition, we demonstrate that the large cytolinker protein plectin localizes only to the cFAs, and a loss of plectin reduces the number of cells possessing this highly unusual FA organization. The presence of plectin within the inner ring of cFAs suggests that they may bear a relationship to hemidesmosomes. However, these FAs are distinct from hemidesmosomes since they contain vinculin, paxillin and talin, while hemidesmosomes do not (Litjens et al., 2006; Ozawa et al., 2010; Tsuruta et al., 2011).

The perinuclear location of the cFAs also indicates a potential relationship to fibrillar adhesions. This is supported by our finding that they contain tensin, a marker of the latter adhesion devices. However, they also contain plectin, paxillin, vinculin and talin. Thus, they are not classical fibrillar adhesions which lack these proteins (Zaidel-Bar et al., 2004; Zamir et al., 1999). Indeed, the unusual location and protein composition of cFAs sets them apart from FAs in other cultured cell types. They appear to belong to a new class of adhesion structures and are distinct from traditional focal complexes, FAs and fibrillar adhesions (Zaidel-Bar et al., 2004; Zamir et al., 1999). Moreover, even the pFAs of primary AEC exhibit unique character. Like the cFAs, pFAs contain the fibrillar adhesion marker tensin, but unlike FAs at the periphery of other cells types, they exhibit little or no dynamic properties (Zamir et al., 2000).

Remarkably, cFAs serve to anchor actin bundles organized into a highly unusual aster-like central array, while the pFAs connect actin filaments parallel along the cell edge. There are few, if any, actin filament connections between pFAs and cFAs making up the outer and inner rings respectively. Moreover, keratin bundles also associate with cFAs in the perinuclear zone, and few keratin bundles are found extending to the cell periphery in cells exhibiting rings of both cFAs and pFAs. Although most rAEC do not display rings of cFAs and pFAs, a decrease in expression of plectin results in a significant decrease in cells displaying the cFA and pFA rings. Indeed, given its ability to link the actin and keratin cytoskeletons, these data suggest that plectin might not only regulate cFA formation into a ring pattern, but may also control the perinuclear organization of both the actin and keratin cytoskeletons in these cells (Seifert et al., 1992; Svitkina et al., 1996; Wiche, 1998).

We were very surprised by the unusual ability of AEC to form the double rings of FAs and the actin aster-like arrangements independent of cell shape since it has been previously reported that distortion of cell size/shape changes the cellular tension and contractility, which in turn alters FA assembly and localization (Chen et al., 2003; Pathak et al., 2008; Théry et al., 2006). Rather, the unique arrangement of cFAs and pFAs in AEC seems to form inherently and is not directly influenced by changes in the aspect ratio, curvature or polarity of the cells. Nonetheless, the formation of both cFAs and the perinuclear actin aster-like array is dependent on actin and myosin-mediated contractility.

cFAs also contribute significantly to the traction forces exerted by rAEC, consistent with their association with the contractile cytoskeleton. Moreover, their formation is dependent on the latter. Indeed, they exhibit properties that make them exquisitely different from FAs located towards the cell interior in other cell

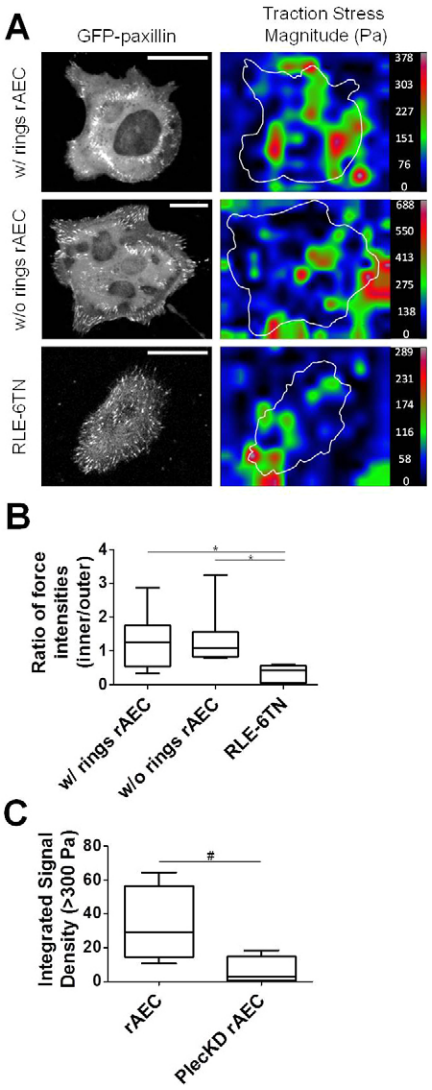

Fig. 6. cFAs in rAEC exert significantly greater internal traction forces than other cells lacking cFAs. (**A**) GFP–paxillin-expressing rAEC and RLE-6TN cells were seeded onto polyacrylamide gels and then processed for traction force analysis. The images on the left show GFP–paxillin, and the images to the right are of reconstructed force maps, demonstrating traction force generation in an individual representative cell. Traction forces are color-coded by traction force stress magnitude as shown on the right (scale shown in Pa). (**B**) Box and whiskers plot of the ratio of forces elicited by at least four pFAs and four cFAs in rAEC exhibiting double FA rings (w/rings) and those without (w/o rings) as well as RLE-6TN cells. The mean force ratio for each cell population (n=7–9 cells each) is indicated by a bar in the boxes; *P<0.05. (**C**) Box and whiskers plot of total traction forces greater than 300 Pa for rAEC and Plec KD rAEC. Loss of plectin results in a decrease in overall traction force. The plot shows the mean integrated signal density for forces >300 Pa for each cell population (n=4–5 cells for each); $^{\#}P$<0.05. Scale bars: 20 µm.

types (Legant et al., 2013; Stricker et al., 2011). Furthermore, we observe no dynamic movement of the cFAs over time, indicating highly stable protein structures, and yet cFAs display significantly faster FRAP turnover rates of GFP–paxillin than pFAs or FAs in cells without the ring pattern. Whether the former property reflects their association with keratin or the central aster-like array of the actin cytoskeleton and what regulates their dynamics will require additional analyses. However, it is tempting to speculate that the unique mechanical environment of the lung exposes AEC to forces not seen by most other cells, leading to the assembly of force-bearing cFAs exhibiting novel cytoskeleton associations (Mead et al., 1970). We suggest that the ability of primary AEC to form their highly unusual FAs likely allows them to resist the tremendous forces to which they are subject in the lung environment (Wirtz and Dobbs, 2000). More detailed analyses in tissues and animal models will be required to test such a hypothesis. Nonetheless, our cell biological analyses have uncovered two types of FAs with unique compositional, structural and functional properties.

Materials and Methods

Alveolar epithelial cell isolation and culture

Protocols for animal studies were approved by the Animal Care and Use Committee of Northwestern University. Primary AEC were isolated from pathogen-free, male Sprague-Dawley rats (200–225 g; for rAEC) or C57/BL6 mice (for mAEC) as previously described (Budinger et al., 2008; DeBiase et al., 2006; Eisenberg et al., 2011). The day of cell isolation is designated as day 0 in culture. On day 2, AEC were removed from plastic dishes using TrypLE Express (Invitrogen; Carlsbad, CA) and replated onto substrates for experiments performed 24–72 hours later, as indicated for each particular assay. Self-assembled monolayer substrates were micropatterned as previously described and coated with 10 µg/ml fibronectin (Sigma; St. Louis, MO) (Chen et al., 1998; Jackman et al., 1995; Kilian et al., 2010). Polyacrylamide gels were prepared as previously using a ratio of 7.5% acrylamide/0.2% bis-acrylamide to generate substrates with a Young's modulus stiffness value measuring about 5 kPa (Eisenberg et al., 2011; Wang and Pelham, 1998). The gels were activated with sulfo-SANPAH according to manufacturer's instructions (Thermo Scientific; Waltham, MA) and also coated with 10 µg/ml fibronectin.

Immortalized cell culture

RLE-6TN (rat lung epithelial, T-antigen negative) and MLE 12 (mouse lung epithelial) cells were gifts from Dr Karen Ridge (Northwestern University). RLE-6TN cells were maintained in Nutrient Mixture F-12 Ham's medium (Sigma-Aldrich) containing 10% fetal bovine serum (FBS) with 2 mM l-glutamine, 100 units/ml penicillin and 100 mg/ml streptomycin. MLE 12 were grown in Minimum Eagle's Medium (Sigma-Aldrich) containing 10% FBS, 4 mM l-glutamine, 100 units/ml penicillin and 100 mg/ml streptomycin. The 804G (rat bladder epithelial) cells have been previously described (Riddelle et al., 1991), as have the immortalized HEK (human epidermal keratinocytes) (Sehgal et al., 2006). Cells were replated onto substrates for experiments performed 24–72 hours later, as indicated for each particular assay.

Antibodies and cytoskeletal drug treatments

The rabbit monoclonal antibodies against plectin (E398P) and paxillin (Y113) were obtained from Epitomics (Burlingame, CA). The mouse monoclonal antibody against β-DG (43DAG1/8D5) was obtained from Abcam Inc. (Cambridge, MA). A polyclonal antibodies against lamin A/C and phosphor-myosin light chain 2 (Thr18/Ser19) were purchased from Cell Signaling Technology (Danvers, MA). The rabbit polyclonal antibody against tensin as well as mouse monoclonal antibodies against vinculin (hVIN-1) and talin (8d4) were obtained from Sigma-Aldrich. The mouse monoclonal antibody against total myosin heavy chain (H11) was a gift from Dr Teng Leong Chew (Northwestern University). A rabbit polyclonal pan-keratin antibody was a gift from Dr Robert D. Goldman (Northwestern University). Rhodamine- and Alexa-Fluor-647-conjugated phalloidin and 4′,6-diamidino-2-phenylindole (DAPI) were purchased from Molecular Probes (Eugene, OR). Horseradish peroxidase (HRP)-conjugated secondary antibodies for western blotting as well as fluorescein isothiocyanate (FITC)- and Rhodamine-labeled secondary antibodies for immunofluorescence were purchased from Jackson ImmunoResearch Laboratories (West Grove, PA).

All chemical inhibitors were from Sigma-Aldrich and made up at a concentration of 1 mg/ml in DMSO, except Y-27632 which was dissolved in double deionized water. Each of the chosen drugs was optimized for the minimal time and amount of drug required to disrupt the respective cytoskeletal target. The drugs and conditions used were: cytochalasin D at 5 µM for 30 minutes, blebbistatin at 50 µM for 30 minutes, nocodazole at 5 µM for 30 minutes, Y-27632 at 10 µM for 60 minutes, and PF-573228 at 10 µM for 3 hours. As a control, cells were treated with diluted DMSO for 30 minutes to 3 hours as appropriate.

Adenoviral infections

For certain experiments, following reattachment, rat cells were infected with adenoviruses encoding short hairpin RNAs (shRNAs) against rat DG, plectin and

human lamin A/C (control) as previously described (Jones et al., 2005; Takawira et al., 2011). AEC were infected with the adenoviruses on day 3, and maximal knockdown of both proteins was obtained 48 hours thereafter, so knock-down assays were conducted on day 5 (about 72 hours after replating) as done previously (Takawira et al., 2011).

Additionally, TFM and live cell experiments were performed using cells infected with a GFP–paxillin-expressing adenovirus. The latter was created using a paxillin/GFP-N plasmid (obtained from Dr Christopher Turner at State University of New York) following standard protocols (Jones et al., 2005; Takawira et al., 2011).

SDS-PAGE and immunoblotting

AEC were solubilized in sample buffer consisting of 8 M urea, 1% sodium dodecyl sulfate in 10 mM Tris-HCl (pH 6.8) and 10% β-mercaptoethanol (Sigma-Aldrich) on day 5 after isolation. Proteins were separated by SDS-PAGE, transferred to nitrocellulose membranes and processed for immunoblotting as previously described (Budinger et al., 2008; Eisenberg et al., 2011). Immunoblots were scanned and quantified using ImageJ (National Institutes of Health, NIH; Bethesda, MD). Results from a minimum of three blots using lysates from at least three independent cell isolations were combined and are presented as the means ± s.e.m.

Immunofluorescence

Substrates were removed from culture media and prepared for immunostaining on day 3–5 after isolation. Two fixation protocols were used to achieve optimal staining. A fixation method using 3.7% formaldehyde in PBS for 5 minutes at room temperature followed by 5 minutes of permeabilization with 0.3% Triton X-100 in PBS was utilized for staining focal adhesion proteins and actin filaments. For stains including plectin or keratin, cells were fixed and extracted with 1:1 mixture of −20℃ acetone and methanol for two minutes and air dried, as previously described (Takawira et al., 2011). Fixed specimens were processed with primary antibodies for 2 hours at 37℃, washed with multiple changes of 5% BSA (BSA; Sigma-Aldrich) in PBS. They were then incubated for 1 hour at room temperature with fluorescently conjugated secondary antibodies. All substrates were extensively washed with 5% BSA in PBS and then mounted onto slides for imaging. Immunofluorescence imaging was performed using a Zeiss UV LSM 510 META laser scanning confocal microscope (Carl Zeiss; Thornwood, NY) with a 63×, 1.4 numerical aperture, oil immersion objective and up to 3× zoom in some panels. Images were exported from the LSM software as tiff files and processed using ImageJ (NIH) and Adobe Photoshop CS2 (Version 9.0, Adobe Systems Inc.; San Jose, CA).

Live-cell imaging of FA dynamics

rAEC infected with adenovirus containing the GFP-paxillin expression vector were used for live-cell imaging of paxillin dynamics and fluorescence recovery after photobleaching (FRAP) experiments. Live images from GFP–paxillin-expressing AEC were captured at 37℃ using a Nikon TE2000 inverted microscope (Nikon Instruments Inc.) with a 60×oil immersion objective every 5 minutes for up to 1 hour using the MetaMorph Imaging System (Universal Imaging, Molecular Devices; Downingtown, PA). All images were then exported as tiff files and analyzed using ImageJ software (NIH). Time-lapse observations for FRAP analyses were made under the following conditions at 37℃: 63×, 1.4 numerical aperture oil immersion objective, maximum power 25 mW, tube current 5.1 A (16% laser power) and pinhole 1.33 airy units (optical slice, 1.0 µm) using a Zeiss UV LSM 510 META laser scanning confocal microscope (Carl Zeiss). Cell regions were bleached at the plane of the membrane at 488 nm, 100% laser power using the minimum number of iterations to cause complete bleaching (50–75 iterations). Recovery was monitored at 16% laser power at 18-second intervals. For quantitative analyses, samples were analyzed using the MBF FRAP profiler plugin for ImageJ software (NIH), and all data were then exported to Microsoft Office Excel 2003 (Microsoft Corporation; Redmond, WA).

Traction force microscopy and analysis

Traction force microscopy was performed on rAEC and RLE-6TN cells cultured on polyacrylamide gel substrates prepared as described above. During gel polymerization, the substrates were impregnated with 1.1 µm red fluorescent beads (Molecular Probes) to serve as fiducial markers for substrate deformation. Live cell imaging was performed using a Nikon A1R laser resonant scanning confocal microscope with a 60×, 1.4 numerical aperture, oil immersion objective and Nikon Elements software (Nikon Instruments Inc.; Melville, NY). Live cell images at room temperature were captured for multiple cells prior to and after cell detachment using TrypLE Express (Invitrogen). These experiments were performed on at least three different occasions, with three cells imaged in two or three samples per day.

Bead displacement analyses were performed by comparing the unstrained bead images obtained after the cells were detached to those bead images where cells remained attached and spread, similar to what has been previously described (Sabass et al., 2008; Stricker et al., 2011; Stricker et al., 2010). Images were exported to ImageJ and aligned using the StackReg plugin (NIH). Iterative Particle Image Velocimetry (PIV) was used to generate a bead displacement field for each set of bead displacement images with the PIV plugin for ImageJ (Tseng, 2011). Then, the force field was reconstructed from this displacement field using the companion FTTC plugin, also for ImageJ (Tseng, 2011). Fluorescence images of each GFP–paxillin-expressing cell was used to identify the x,y location of cFAs and pFAs for each cell. These locations were identified on the reconstructed force field, and their corresponding force magnitudes were tabulated for specific FAs identified as inner (>5 µm inward from cell edge) and outer (within 5 µm of cell edge) within a given cell. In order to compensate for slight cell-to-cell variations in overall traction force, the sum of forces attributable to a given number of inner FAs was determined relative to the sum of forces attributable to an equal number of outer FAs. Therefore, a force ratio close to 1 indicates that the inner and outer FAs are exerting similar traction forces in a given cell. At least four inner and four outer FAs were used for quantitative analysis from $n=7$–9 cells per type. For traction forces within rAEC and Plec KD rAEC, the integrated signal density was determined for traction forces greater than 300 Pa. Traction force data are presented as box and whiskers plots made using GraphPad Prism software (Version 3.0, GraphPad Software; La Jolla, CA).

Statistical analysis

Significant differences between experimental conditions were explored with either one-way ANOVA testing with Tukey's comparison analyses or the two-tailed, paired Student's *t*-test using GraphPad Prism software. A significant difference was identified as $P<0.05$.

Acknowledgements

We thank Drs Robert D. Goldman, Karen Ridge, Christopher S. Turner and Kevin J. Hamill for their gifts of antibodies, cells, reagents and help with data analyses, respectively. Isolation of AEC was performed by the Pulmonary Division Core B Facility in compliance with proper guidelines outlined by the Institutional Animal Care and Use Committee. Microscopy was performed at the Northwestern University Cell Imaging Facility supported by NCI-CCSG-P30-CA060553 awarded to the Robert H. Lurie Comprehensive Cancer Center.

Author contributions

J.L.E. and J.C.R.J. designed experiments and wrote the manuscript. J.L.E., K.G.B. and D.T. carried out experimental work. J.L.E. and K.G.B. analyzed data. S.B.H. generated plasmid constructs. J.L.E., K.G.B., M.M., G.R.S.B. and J.C.R.J. participated in experimental design and provided scientific advice.

Funding

This work was supported by a training grant from the National Heart, Lung and Blood Institute [grant number T32HL076139 to J.L.E.]; the American Heart Association Midwest affiliate postdoctoral training program [grant number 12POST8610002 to J.L.E.]; and the National Institutes of Health [grant number RO1HL092963 to J.C.R.J. and G.R.S.B.]; the National Cancer Institute [grant number U54CA151880 to M.M.]; and the Chicago Biomedical Consortium with support from the Searle Funds at the Chicago Community Trust [grant number C2006-00997 to M.M.]. Deposited in PMC for release after 12 months.

Supplementary material available online at
http://jcs.biologists.org/lookup/suppl/doi:10.1242/jcs.128975/-/DC1

References

Berrier, A. L. and Yamada, K. M. (2007). Cell-matrix adhesion. *J. Cell. Physiol.* **213**, 565-573.

Bhadriraju, K., Yang, M., Alom Ruiz, S., Pirone, D., Tan, J. and Chen, C. S. (2007). Activation of ROCK by RhoA is regulated by cell adhesion, shape, and cytoskeletal tension. *Exp. Cell Res.* **313**, 3616-3623.

Bhattacharya, R., Gonzalez, A. M., Debiase, P. J., Trejo, H. E., Goldman, R. D., Flitney, F. W. and Jones, J. C. (2009). Recruitment of vimentin to the cell surface by beta3 integrin and plectin mediates adhesion strength. *J. Cell Sci.* **122**, 1390-1400.

Brock, A., Chang, E., Ho, C. C., LeDuc, P., Jiang, X., Whitesides, G. M. and Ingber, D. E. (2003). Geometric determinants of directional cell motility revealed using microcontact printing. *Langmuir* **19**, 1611-1617.

Budinger, G. R., Urich, D., DeBiase, P. J., Chiarella, S. E., Burgess, Z. O., Baker, C. M., Soberanes, S., Mutlu, G. M. and Jones, J. C. (2008). Stretch-induced activation of AMP kinase in the lung requires dystroglycan. *Am. J. Respir. Cell Mol. Biol.* **39**, 666-672.

Burgstaller, G., Gregor, M., Winter, L. and Wiche, G. (2010). Keeping the vimentin network under control: cell-matrix adhesion-associated plectin 1f affects cell shape and polarity of fibroblasts. *Mol. Biol. Cell* **21**, 3362-3375.

Burridge, K. and Chrzanowska-Wodnicka, M. (1996). Focal adhesions, contractility, and signaling. *Annu. Rev. Cell Dev. Biol.* **12**, 463-518.

Burridge, K., Fath, K., Kelly, T., Nuckolls, G. and Turner, C. (1988). Focal adhesions: transmembrane junctions between the extracellular matrix and the cytoskeleton. *Annu. Rev. Cell Biol.* **4**, 487-525.

Chen, C. S., Mrksich, M., Huang, S., Whitesides, G. M. and Ingber, D. E. (1997). Geometric control of cell life and death. *Science* **276**, 1425-1428.

Chen, C. S., Mrksich, M., Huang, S., Whitesides, G. M. and Ingber, D. E. (1998). Micropatterned surfaces for control of cell shape, position, and function. *Biotechnol. Prog.* **14**, 356-363.

Chen, C. S., Alonso, J. L., Ostuni, E., Whitesides, G. M. and Ingber, D. E. (2003). Cell shape provides global control of focal adhesion assembly. *Biochem. Biophys. Res. Commun.* **307**, 355-361.

DeBiase, P. J., Lane, K., Budinger, S., Ridge, K., Wilson, M. and Jones, J. C. (2006). Laminin-311 (Laminin-6) fiber assembly by type I-like alveolar cells. *J. Histochem. Cytochem.* **54**, 665-672.

Dike, L. E., Chen, C. S., Mrksich, M., Tien, J., Whitesides, G. M. and Ingber, D. E. (1999). Geometric control of switching between growth, apoptosis, and differentiation during angiogenesis using micropatterned substrates. *In Vitro Cell. Dev. Biol. Anim.* **35**, 441-448.

Eisenberg, J. L., Safi, A., Wei, X., Espinosa, H. D., Budinger, G. S., Takawira, D., Hopkinson, S. B. and Jones, J. C. (2011). Substrate stiffness regulates extracellular matrix deposition by alveolar epithelial cells. *Res. Rep. Biol.* **2011**, 1-12.

Geerts, D., Fontao, L., Nievers, M. G., Schaapveld, R. Q., Purkis, P. E., Wheeler, G. N., Lane, E. B., Leigh, I. M. and Sonnenberg, A. (1999). Binding of integrin alpha6beta4 to plectin prevents plectin association with F-actin but does not interfere with intermediate filament binding. *J. Cell Biol.* **147**, 417-434.

Geiger, B. and Bershadsky, A. (2001). Assembly and mechanosensory function of focal contacts. *Curr. Opin. Cell Biol.* **13**, 584-592.

Geiger, T. and Zaidel-Bar, R. (2012). Opening the floodgates: proteomics and the integrin adhesome. *Curr. Opin. Cell Biol.* **24**, 562-568.

Geiger, B., Spatz, J. P. and Bershadsky, A. D. (2009). Environmental sensing through focal adhesions. *Nat. Rev. Mol. Cell Biol.* **10**, 21-33.

Gonzales, M., Weksler, B., Tsuruta, D., Goldman, R. D., Yoon, K. J., Hopkinson, S. B., Flitney, F. W. and Jones, J. C. (2001). Structure and function of a vimentin-associated matrix adhesion in endothelial cells. *Mol. Biol. Cell* **12**, 85-100.

Hamill, K. J., Hopkinson, S. B., DeBiase, P. and Jones, J. C. (2009). BPAG1e maintains keratinocyte polarity through beta4 integrin-mediated modulation of Rac1 and cofilin activities. *Mol. Biol. Cell* **20**, 2954-2962.

Jackman, R. J., Wilbur, J. L. and Whitesides, G. M. (1995). Fabrication of submicrometer features on curved substrates by microcontact printing. *Science* **269**, 664-666.

James, J., Goluch, E. D., Hu, H., Liu, C. and Mrksich, M. (2008). Subcellular curvature at the perimeter of micropatterned cells influences lamellipodial distribution and cell polarity. *Cell Motil. Cytoskeleton* **65**, 841-852.

Jones, J. C., Lane, K., Hopkinson, S. B., Lecuona, E., Geiger, R. C., Dean, D. A., Correa-Meyer, E., Gonzales, M., Campbell, K., Sznajder, J. I. et al. (2005). Laminin-6 assembles into multimolecular fibrillar complexes with perlecan and participates in mechanical-signal transduction via a dystroglycan-dependent, integrin-independent mechanism. *J. Cell Sci.* **118**, 2557-2566.

Karashima, T., Tsuruta, D., Hamada, T., Ishii, N., Ono, F., Hashikawa, K., Ohyama, B., Natsuaki, Y., Fukuda, S., Koga, H. et al. (2012). Interaction of plectin and intermediate filaments. *J. Dermatol. Sci.* **66**, 44-50.

Kilian, K. A., Bugarija, B., Lahn, B. T. and Mrksich, M. (2010). Geometric cues for directing the differentiation of mesenchymal stem cells. *Proc. Natl. Acad. Sci. USA* **107**, 4872-4877.

Lawson, C., Lim, S. T., Uryu, S., Chen, X. L., Calderwood, D. A. and Schlaepfer, D. D. (2012). FAK promotes recruitment of talin to nascent adhesions to control cell motility. *J. Cell Biol.* **196**, 223-232.

Legant, W. R., Choi, C. K., Miller, J. S., Shao, L., Gao, L., Betzig, E. and Chen, C. S. (2013). Multidimensional traction force microscopy reveals out-of-plane rotational moments about focal adhesions. *Proc. Natl. Acad. Sci. USA* **110**, 881-886.

Litjens, S. H., de Pereda, J. M. and Sonnenberg, A. (2006). Current insights into the formation and breakdown of hemidesmosomes. *Trends Cell Biol.* **16**, 376-383.

Liu, M., Tanswell, A. K. and Post, M. (1999). Mechanical force-induced signal transduction in lung cells. *Am. J. Physiol.* **277**, L667-L683.

McBeath, R., Pirone, D. M., Nelson, C. M., Bhadriraju, K. and Chen, C. S. (2004). Cell shape, cytoskeletal tension, and RhoA regulate stem cell lineage commitment. *Dev. Cell* **6**, 483-495.

Mead, J., Takishima, T. and Leith, D. (1970). Stress distribution in lungs: a model of pulmonary elasticity. *J. Appl. Physiol.* **28**, 596-608.

Na, S., Chowdhury, F., Tay, B., Ouyang, M., Gregor, M., Wang, Y., Wiche, G. and Wang, N. (2009). Plectin contributes to mechanical properties of living cells. *Am. J. Physiol.* **296**, C868-C877.

Ostuni, E., Whitesides, G. M., Ingber, D. E. and Chen, C. S. (2009). Using self-assembled monolayers to pattern ECM proteins and cells on substrates. *Methods Mol. Biol.* **522**, 183-194.

Ozawa, T., Tsuruta, D., Jones, J. C., Ishii, M., Ikeda, K., Harada, T., Aoyama, Y., Kawada, A. and Kobayashi, H. (2010). Dynamic relationship of focal contacts and hemidesmosome protein complexes in live cells. *J. Invest. Dermatol.* **130**, 1624-1635.

Pathak, A., Deshpande, V. S., McMeeking, R. M. and Evans, A. G. (2008). The simulation of stress fibre and focal adhesion development in cells on patterned substrates. *J. R. Soc. Interface* **5**, 507-524.

Riddelle, K. S., Green, K. J. and Jones, J. C. (1991). Formation of hemidesmosomes in vitro by a transformed rat bladder cell line. *J. Cell Biol.* **112**, 159-168.

Riveline, D., Zamir, E., Balaban, N. Q., Schwarz, U. S., Ishizaki, T., Narumiya, S., Kam, Z., Geiger, B. and Bershadsky, A. D. (2001). Focal contacts as mechanosensors: externally applied local mechanical force induces growth of focal contacts by an mDia1-dependent and ROCK-independent mechanism. *J. Cell Biol.* **153**, 1175-1186.

Sabass, B., Gardel, M. L., Waterman, C. M. and Schwarz, U. S. (2008). High resolution traction force microscopy based on experimental and computational advances. *Biophys. J.* **94**, 207-220.

Sehgal, B. U., DeBiase, P. J., Matzno, S., Chew, T. L., Claiborne, J. N., Hopkinson, S. B., Russell, A., Marinkovich, M. P. and Jones, J. C. (2006). Integrin beta4 regulates migratory behavior of keratinocytes by determining laminin-332 organization. *J. Biol. Chem.* **281**, 35487-35498.

Seifert, G. J., Lawson, D. and Wiche, G. (1992). Immunolocalization of the intermediate filament-associated protein plectin at focal contacts and actin stress fibers. *Eur. J. Cell Biol.* **59**, 138-147.

Stricker, J., Sabass, B., Schwarz, U. S. and Gardel, M. L. (2010). Optimization of traction force microscopy for micron-sized focal adhesions. *J. Phys. Condens. Matter* **22**, 194104.

Stricker, J., Aratyn-Schaus, Y., Oakes, P. W. and Gardel, M. L. (2011). Spatiotemporal constraints on the force-dependent growth of focal adhesions. *Biophys. J.* **100**, 2883-2893.

Svitkina, T. M., Verkhovsky, A. B. and Borisy, G. G. (1996). Plectin sidearms mediate interaction of intermediate filaments with microtubules and other components of the cytoskeleton. *J. Cell Biol.* **135**, 991-1007.

Takawira, D., Budinger, G. R., Hopkinson, S. B. and Jones, J. C. (2011). A dystroglycan/plectin scaffold mediates mechanical pathway bifurcation in lung epithelial cells. *J. Biol. Chem.* **286**, 6301-6310.

Théry, M., Pépin, A., Dressaire, E., Chen, Y. and Bornens, M. (2006). Cell distribution of stress fibres in response to the geometry of the adhesive environment. *Cell Motil. Cytoskeleton* **63**, 341-355.

Tseng, O. (2011). *Study of Multicellular Architecture With Controled Environment*. PhD dissertation, Universite de Genoble, Grenoble, France.

Tsuruta, D., Gonzales, M., Hopkinson, S. B., Otey, C., Khuon, S., Goldman, R. D. and Jones, J. C. (2002). Microfilament-dependent movement of the beta3 integrin subunit within focal contacts of endothelial cells. *FASEB J.* **16**, 866-868.

Tsuruta, D., Hashimoto, T., Hamill, K. J. and Jones, J. C. (2011). Hemidesmosomes and focal contact proteins: functions and cross-talk in keratinocytes, bullous diseases and wound healing. *J. Dermatol. Sci.* **62**, 1-7.

Wang, Y. L. and Pelham, R. J., Jr (1998). Preparation of a flexible, porous polyacrylamide substrate for mechanical studies of cultured cells. *Methods Enzymol.* **298**, 489-496.

Wiche, G. (1998). Role of plectin in cytoskeleton organization and dynamics. *J. Cell Sci.* **111**, 2477-2486.

Windoffer, R., Kölsch, A., Wöll, S. and Leube, R. E. (2006). Focal adhesions are hotspots for keratin filament precursor formation. *J. Cell Biol.* **173**, 341-348.

Wirtz, H. R. and Dobbs, L. G. (2000). The effects of mechanical forces on lung functions. *Respir. Physiol.* **119**, 1-17.

Zaidel-Bar, R., Cohen, M., Addadi, L. and Geiger, B. (2004). Hierarchical assembly of cell-matrix adhesion complexes. *Biochem. Soc. Trans.* **32**, 416-420.

Zaidel-Bar, R., Itzkovitz, S., Ma'ayan, A., Iyengar, R. and Geiger, B. (2007). Functional atlas of the integrin adhesome. *Nat. Cell Biol.* **9**, 858-867.

Zamir, E. and Geiger, B. (2001). Molecular complexity and dynamics of cell-matrix adhesions. *J. Cell Sci.* **114**, 3583-3590.

Zamir, E., Katz, B. Z., Aota, S., Yamada, K. M., Geiger, B. and Kam, Z. (1999). Molecular diversity of cell-matrix adhesions. *J. Cell Sci.* **112**, 1655-1669.

Zamir, E., Katz, M., Posen, Y., Erez, N., Yamada, K. M., Katz, B. Z., Lin, S., Lin, D. C., Bershadsky, A., Kam, Z. et al. (2000). Dynamics and segregation of cell-matrix adhesions in cultured fibroblasts. *Nat. Cell Biol.* **2**, 191-196.

Journal of Cell Science

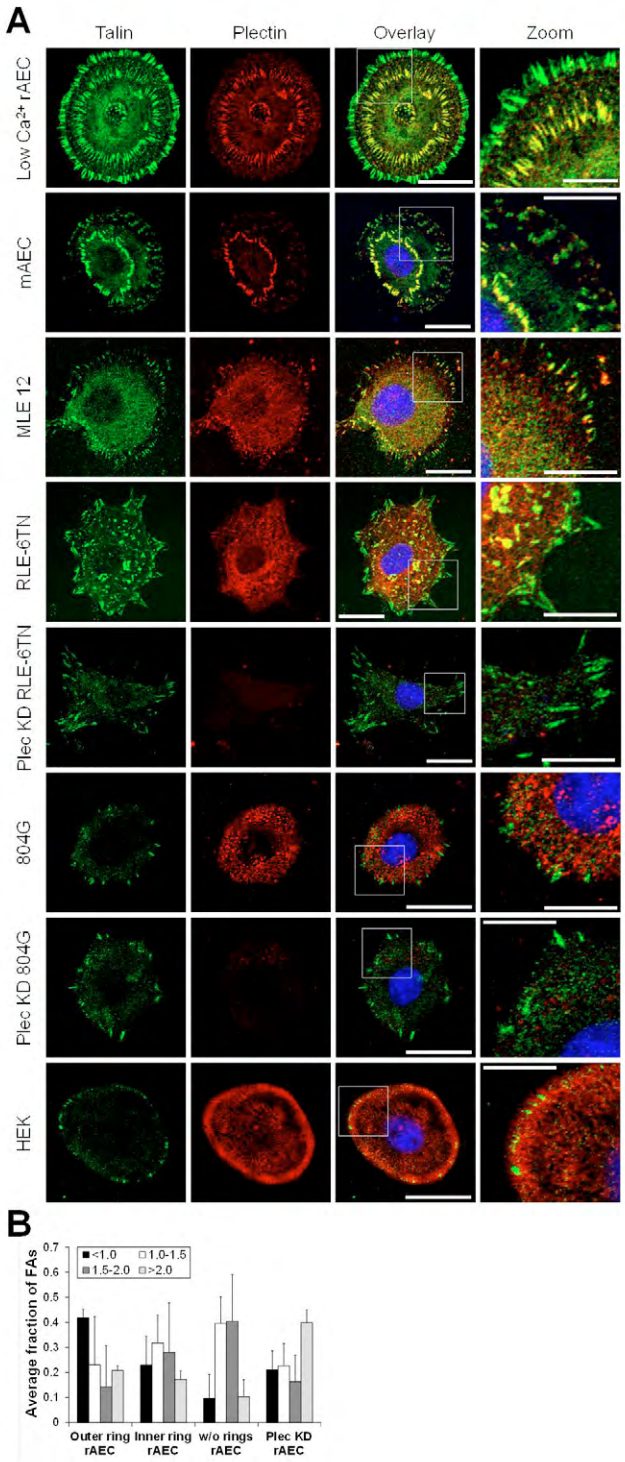

Fig. S1. FA organization in AEC and additional cell types. (A) Immunostaining for talin and plectin was performed on the cells types indicated on the left of the images and conditions as marked. The overlays of the two images on the left are shown in the third column and include nuclear DAPI staining shown in blue if present. The boxed areas in the overlays are shown at higher magnifications in the right column (zoom). Scale bars: 20 μm in the overlay; 10 μm in zoom. (B) The graph presents the average number of FAs within the designated size range out of the total number of FAs measured for each cell type; n≥25 FAs in 3-6 cells per condition ± s.d.

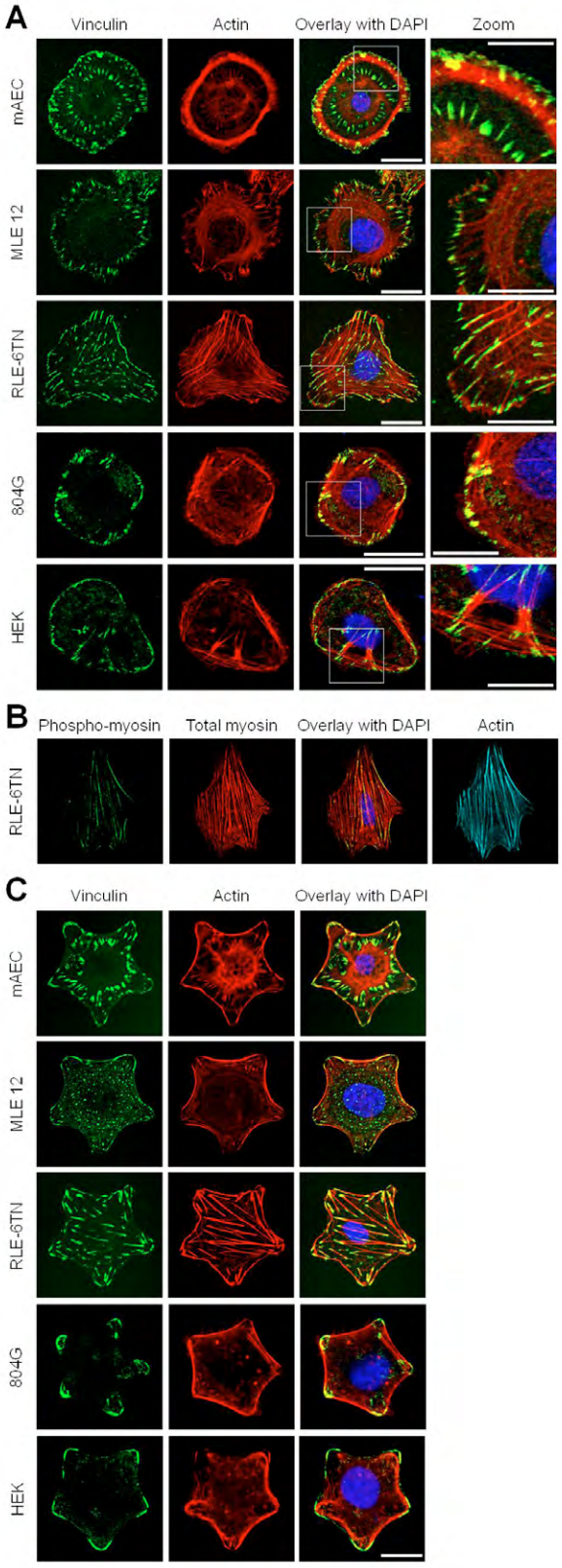

Fig. S2. Actin organization in AEC and other epithelial cell types. (A) FAs of the indicated cells were stained using an antibody against vinculin together with Rhodamine-conjugated phalloidin as a marker for actin. Overlays of the two images on the left are shown in the third column and include DAPI staining of nuclei. The boxed areas in the overlays are shown at higher magnifications (zoom) in the column at the right. Scale bars: 20 μm in overlay; 10 μm in zoom. (B) RLE-6TN plated on glass coverslips were immunostained for phospho- and total-myosin and also processed with Alexa647-conjugated phalloidin to mark the actin cytoskeleton. Overlays of the two images on the left are shown in the third column and include DAPI staining of nuclei. The images in the right column show the total actin cytoskeletal network. Scale bar: 20 μm. (C) The indicated cells were seeded onto star micro-patterns and stained for vinculin and actin. Overlays of the two images on the left are shown in the third column and include DAPI nuclear staining. Scale bar: 20 μm.

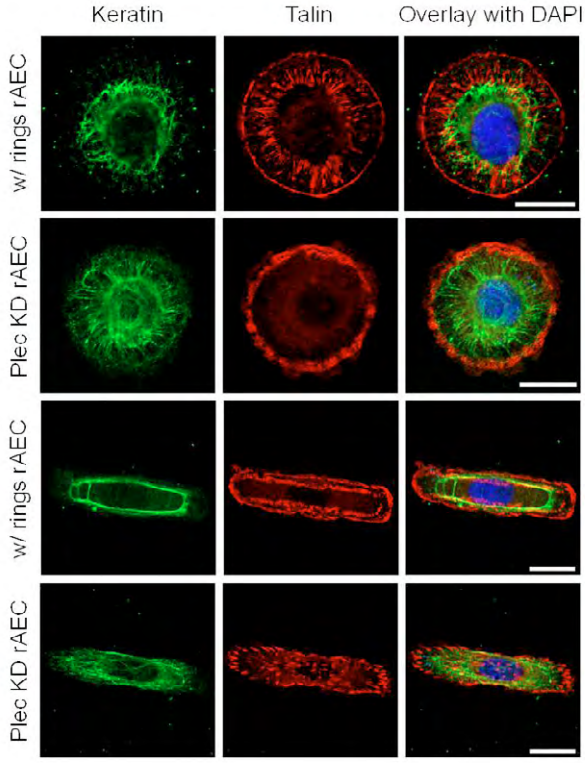

Fig. S3. Keratin bundles are restricted by cFA rings when cells are plated onto micro-patterned substrates. rAEC and Plec KD rAEC maintained on circle or rectangle micro-patterned substrates were immunostained for keratin and talin. The overlay of the two images to the left is shown in the right column and includes DAPI staining of nuclei. Scale bar: 20 μm.

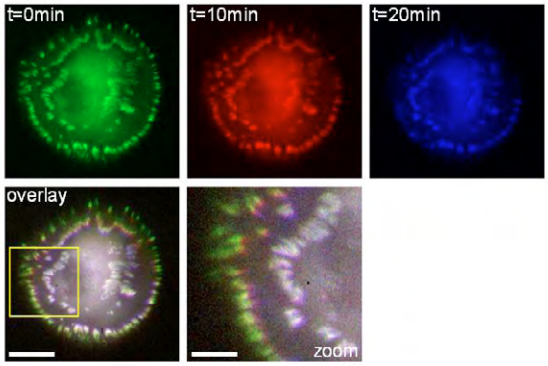

Fig. S4. pFAs and cFAs in rAEC display minimal dynamics. Live images of rAEC infected with GFP-paxillin were captured over time. Three of the resulting images (t=0, 10, and 20 min) were labeled in green, red, and blue colors respectively, and the three images were overlaid to display FA dynamics. The white color in the overlay and zoom images (scale bars: 20 μm and 10 μm respectively) indicates lack of movement.